Forest Biomass Estimation Using Texture Measurements of High-Resolution Dual-Polarization C-Band SAR Data

Md. Latifur Rahman Sarker, Janet Nichol, Huseyin Baki Iz, Baharin Bin Ahmad, and Alias Abdul Rahman

***Abstract*—Recent synthetic aperture radar (SAR) sensors with a capability of providing data with varying spatial resolutions, polarizations, and incidence angles have attracted greater interest for forest biomass and carbon storage estimation. This study investigates the capability of RADARSAT-2 fine-beam dual-polarization (C-HV and C-HH) data for forest biomass estimation in complex subtropical forest, with different types of processing: 1) raw intensity data (both polarizations separately and as polarization ratio) and 2) texture parameters of both polarizations (separately, jointly, and as polarization ratio). Field data (diameter at breast height and height) were collected from 53 field plots and converted to biomass (dry weight) using a newly developed allometric model. Finally, biomass estimation models were developed between SAR signatures from different processing steps and field plot biomass using stepwise multiple regression. All biomass estimation models using radar intensity data (C-HV, C-HH, and ratio of C-HV and C-HH) proved ineffective, but texture parameters derived from intensity data showed potential. We were able to estimate forest biomass amounts up to 360 t/ha with a goodness of fit of 0.78 (adjusted r^2) and an rmse of 28.68 t/ha using the combination of texture parameters of both polarizations (C-HV and C-HH). However, goodness of fit could be improved to 0.91 (adjusted r^2) and an rmse of 26.95 t/ha for biomass levels up to 532 t/ha using the ratio of texture parameters of C-HV/C-HH. The result is very encouraging and indicates that the dual-polarization C-band SAR sensor has a potential for the estimation of forest biomass, particularly using the polarization ratio of texture measurements, and biomass estimation can be improved substantially beyond the previously stated saturation level for C-band SAR.**

***Index Terms*—Carbon storage capacity, forest biomass, RADARSAT-2, texture measurement, texture ratio.**

Manuscript received July 29, 2011; revised March 19, 2012 and July 15, 2012; accepted August 30, 2012. Date of publication November 16, 2012; date of current version May 16, 2013. This work was supported in part by the Hong Kong Research Grants Council under General Research Fund Grant PolyU5281/09E and in part by Universiti Teknologi Malaysia under Grant FAVF-4D059.

M. L. R. Sarker is with the Department of Remote Sensing, Universiti Teknologi Malaysia, Johor Bahru 81310, Malaysia, and also with the Department of Geography and Environmental Studies, University of Rajshahi, Rajshahi 6100, Bangladesh (e-mail: lrsarker@yahoo.com).

J. Nichol and H. B. Iz are with the Department of Land Surveying and Geo-Informatics, The Hong Kong Polytechnic University, Kowloon, Hong Kong (e-mail: lsjanet@inet.polyu.edu.hk; lshbiz@inet.polyu.edu.hk).

B. B. Ahmad is with the Department of Remote Sensing, Universiti Teknologi Malaysia, Johor Bahru 81310, Malaysia (e-mail: baharinahmad@utm.my).

A. A. Rahman is with the Department of Geoinformatics, Universiti Teknologi Malaysia, Johor Bahru 81310, Malaysia (e-mail: alias@utm.my).

Color versions of one or more of the figures in this paper are available online at http://ieeexplore.ieee.org.

Digital Object Identifier 10.1109/TGRS.2012.2219872

I. Introduction

ESTIMATION of forest biomass at regional and global scales is essential for understanding and monitoring ecosystem response to climate change for greenhouse gas inventories, terrestrial carbon accounting, and climate change modeling [1]–[4]. Traditional methods of forest biomass estimation are the most accurate but are time consuming and destructive and, as a result, are limited only to small areas [5]. Remote sensing offers an effective alternative method for forest biomass and carbon inventory at local, regional, and global scales [6], [7]. Studies have been conducted for forest biomass estimation using optical sensors [8]–[12], synthetic aperture radar (SAR) sensors [13]–[18], Lidar [19], and multisensors [20], [21] with varying degrees of success.

Among the different types of sensors, SAR shows great potential for forest biomass estimation because of its sensitivity to the plant canopy coupled with penetration ability [7]. Past studies have indicated that L-band cross polarization (L-HV) is the most suitable available choice (as no P-band spaceborne SAR is planned), but C-band SAR is also effective for less woody biomass. Research works [1], [2], [7], [22] have shown that, on average, C-band data saturate below 50 t/ha, L-band data saturate at less than 100t/ha, and P-band data saturate at less than 200 t/ha of biomass.

The new generation of spaceborne SAR sensors, i.e., L-band PALSAR (no longer operational), C-band RADARSAT-2, X-band TerraSAR, and Cosmo Skymed, has provided new opportunities for forest biomass estimation using SAR because of the ability to provide data with varying spatial resolutions, polarizations, and incidence angles. Although the new SAR data are more attractive than the previous generation of spaceborne SAR, i.e., JERS-1, ERS-1/-2, and RADARSAT-1, previous studies indicated that improvement of forest biomass estimation not only depends on the SAR data but also requires effective SAR data processing [22] such as texture measurement. Texture measurement is the most important source of information in high-resolution SAR images [23], [24], and image texture is capable of identifying different aspects of forest stand structure, including age, density, and leaf area index [25].

Texture is a function of local variance in the image which is related to the spatial resolution and the size of the dominant scene objects [26]. In forested landscapes, texture is dependent on the size and spacing of tree crowns, such that, on

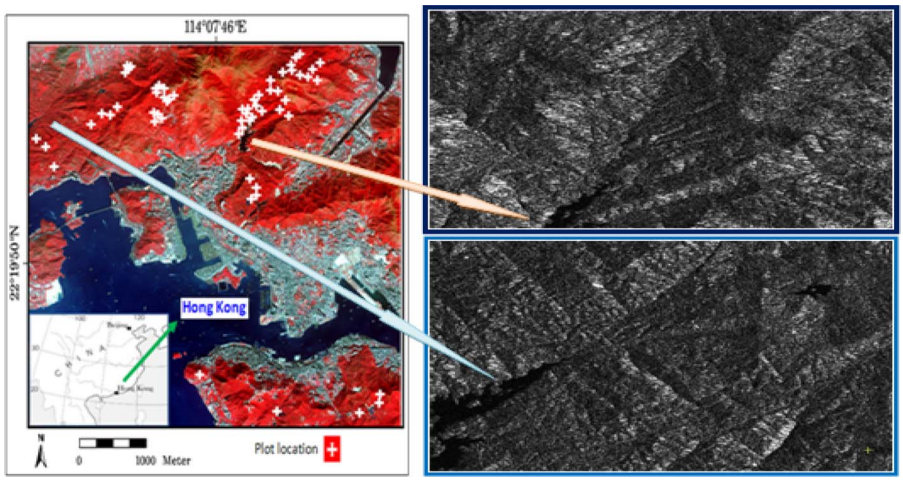

Fig. 1. Study area and distribution of field plots.

high-resolution images, if a pixel falls on a tree, its neighbor may also fall on the same tree, resulting in a low local variance. As the resolution increases to a level comparable to the dominant tree crown size, local variance increases, and this should be particularly true in tropical forests with high species diversity where stands are heterogeneous [27]. The advantage of texture is that it can maximize the discrimination of spatial information independently of tone (i.e., backscatter), and this potentially increases the biomass range that can be measured with SAR data by increasing the saturation level [28], [29]. Previous research indicates that texture parameters are very useful for land cover and vegetation classification [30], [31], but image texture and its relation with forest biomass have not yet been fully investigated [17], [25], [28] probably due to the difficulty of selecting appropriate texture measures along with window size [32], [33] as well as the previous unavailability of high-resolution spaceborne SAR which is believed to be a source of better texture information in SAR images [28].

However, considering the necessity of forest biomass estimation and the opportunity to investigate texture measurement in combination with the data from new SAR sensors, this paper examines advanced SAR (RADARSAT-2) data for forest biomass estimation using different types of texture parameters and processing techniques. The C-band RADARSAT-2 SAR was selected because the L-band PALSAR is no longer available and Cosmo Skymed and TerraSAR are X-band. Although RADARSAT-2 uses C-band, it can provide data with different polarizations with varying incidence angles as well as high spatial resolution, and our approach is to utilize the benefits of spatial resolution and wavelength, considering the observations of previous studies [28], [34], [35] about RADARSAT-2; all of which mentioned that C-band SAR can provide excellent texture properties for biomass estimation when it is acquired at a high spatial resolution.

A. Objectives

This paper aims to improve the estimation of forest biomass using SAR data. Other more specific objectives are the following: 1) to develop an allometric model which will be useful for future biomass estimation in Hong Kong and other places in the subtropical evergreen forest zone; 2) to investigate the efficiency of SAR intensity and SAR texture parameters of both polarizations individually, jointly, and as a ratio for the estimation of forest biomass; 3) to investigate the different types of texture measurements of SAR data both individually and jointly for forest biomass estimation; and 4) to find a best fit model for forest biomass estimation using multiscale texture measurement of high-resolution dual-polarization C-band SAR.

II. Study Area and Data

A. Study Area and Forest

The study area for this research is the Hong Kong Special Administrative Region (Fig. 1) which lies on the southeast coast of China and just south of the Tropic of Cancer. The total land area of Hong Kong is 1100 km^2 which includes 235 small outlying islands. Approximately 40% of the total area is designated as country parks which are reserved for natural vegetation under the management of the Agriculture, Fisheries and Conservation Department (AFCD).

The forests of Hong Kong were subtropical, dense, and lush, dominated by evergreen trees belonging to the oak and laurel families. By the late 1940s, Hong Kong was largely barren and without trees due to the widespread cutting of fuel during the Second World War. However, during the 1950s, 1960s, 1970s, and up to the early 1980s, hardy and fast-growing pioneer species such as Chinese Red Pine, Acacia, and Brisbane Box were widely planted. Because of the extensive tree plantation of native and nonnative (including Machilus species, Lophostemon, Eucalyptus species, Acacia species, Pine, Castonopisis, and Malaluca), prohibition of tree cutting, and the natural growth of new young forests, the forest succession is ongoing. As a result, the native subtropical evergreen broad leaf forest has been replaced by a complex patchwork of regenerating secondary forest in various stages of development and plantations.

B. Data

A dual-polarization (HV and HH) C-band fine-beam image (January 1, 2009) from the RADARSAT-2 SAR satellite image with approximate resolution of 10.4 to 6.8 m in range and

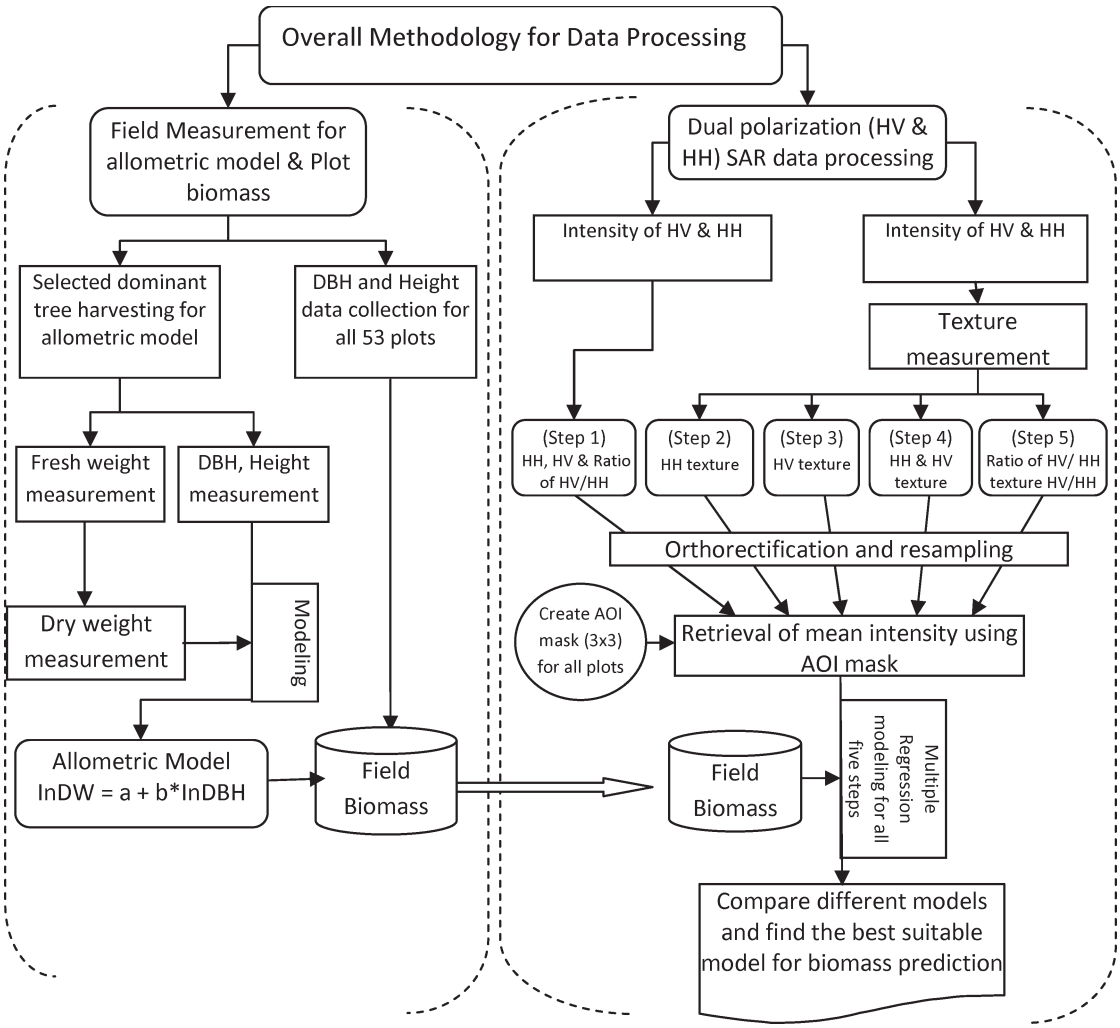

Fig. 2. Overall methodology.

7.7 m in azimuth directions was used in this study. The incidence angle of the data was 34.2°.

III. Methodology

This study comprises two parts, i.e., allometric model development for field biomass and SAR image processing (Fig. 2). Field measurement of DBH and height was carried out in 53 plots, and the field DBH data were converted into field biomass using a newly developed allometric model. SAR intensity data were converted into backscattering coefficient, and texture measurements were carried out for each polarization. After geometric correction, all texture parameters were divided into five processing groups: 1) intensity images (HV and HH individually and as ratio); 2) texture parameters of HV polarization; 3) texture parameters of HH polarization; 4) texture parameters of HV and HH polarizations jointly; and 5) ratio of texture parameters of HV and HH polarizations. The mean intensity of SAR data was extracted using an area of interest mask corresponding to the 53 field plots, and multiple linear regression was performed between SAR parameters and field plot biomass. The aforementioned methodology is detailed in the following.

A. Allometric Model Development

The complex history of Hong Kong forest makes it difficult to find an effective existing allometric model which includes a representative sample of trees. Therefore, an allometric model was developed by harvesting 75 trees (from 14 dominant species) in four DBH classes (less than 10 cm, 10–15 cm, 15–20 cm, and 20 cm and above). The harvested trees were separated into fractions including leaves, twigs, small branches, large branches, and stem. The measurements of DBH, height, fresh weight, and dry weight (DW) were taken for all harvested trees following the procedures of previous studies [5], [6], [36]. Tree parameters such as DBH and DW were used for the development of the allometric model considering DW as the dependent variable and DBH and height as independent variables. Twelve regression models used by previous researchers [6], [36], [37] were tested, and the best fit model ($\mathrm{InDW} = a + b * \mathrm{InDBH}$) was found using the log-transformed DBH and DW as dependent and independent variables, respectively, in the least square regression model. The bias of the model was corrected according to Baskerville's method [38] multiplying by the correction factor "exp (mse/2 or $S_{\varepsilon}^2/2$)." The performance of the allometric model (Table I) was highly

TABLE I
BEST FIT ALLOMETRIC MODEL

Regression Model	Coefficient & Value		Std Err. of Coef.	CF (mse/2)	r^2_{adj}	Fit index (FI)	RMSE (kg)	p
$\widehat{DW} = e^a DBH^b e^{mse/2}$	a	-2.057	0.183	0.021	0.93	0.90	13.52	0.0005
	b	2.289	0.072					

TABLE II
FIELD BIOMASS/DW DISTRIBUTION IN GENERAL AND BASED ON PLOT SETTINGS

Dry weight (DW) class (in t/ha)		Number of plots	Percentage
Less than 100		13	24.53
100 - 150		19	35.85
150 -200		13	24.53
200 & above		8	15.09
Biomass/dry weight level of 53 plot settings		Biomass/dry weight level of 45 plot settings	
Biomass/dry weight class (t/ha)	Biomass/dry weight (t/ha)	Biomass/dry weight class (t/ha)	Biomass/dry weight (t/ha)
Less than 100	51.04, 77.46,78.11, 82.38, 83.24, 83.33, 83.87, 84.48, 92.16, 93.46, 94.68, 95.87, 98.06	Less than 100	51.04, 77.46, 78.11, 82.38, 83.24, 83.87, 92.16, 95.87, 98.06
100 - 150	102.23, 104.60,107.04 108.10, 109.39,110.98 111.67,120.36,122.96 123.11,124.13,131.55 133.36,136.20,138.04 141.90,146.02,147.49 149.64	100 - 150	102.23,104.60,109.39 110.98,111.67,120.36 122.96,123.11,124.13 131.55,133.36,136.20 138.04,141.90,146.02 147.49,149.64
150 -200	151.46,156.69,157.44 157.59,163.14,166.56 166.70,177.49,178.49 178.89,183.81,188.62 189.35	150 -200	151.46,156.69,157.44 157.59,163.14,166.56 166.70,177.49,178.49 178.89,183.81,188.62 189.35
200 & above	229.73,270.88,311.39 312.05,317.93,360.84 518.60,532.09	200 & above	229.73,270.88,311.39 312.05,317.93,360.84

satisfactory considering the adjusted r^2 (0.93), fit index (0.90), rmse (13.52 t/ha), and p-value (0.0005), and in view of the great variety of tree species, this performance is similar to that of several other studies [6], [36].

B. Field Plot Measurement and Field Biomass Estimation

Because forest area of Hong Kong is mostly inaccessible due to topographic conditions, random or stratified sampling could not be used for field plot selection. Therefore, after field investigation and consultation with AFCD ecologists, purposive sampling was conducted for the selection of 53 field plots to cover a variety of tree stands (from low to high biomass), and all the plots were established on flat and steady slope areas avoiding rugged terrain. Circular plots with a 15-m radius were determined considering the image resolution, orthorectification error, and GPS positioning error, and plots were positioned within a homogeneous area of forest and at least 15 m distant from other features such as roads, water bodies, and other infrastructure. A Leica GS5+ GPS was used to determine the center of each plot using Differential Global Positioning System (DGPS) mode for accuracy within ± 3 m. Both DBH and tree height were measured for all trees within the circular plot region. The measured DBH of each tree as well as each plot was converted into plot biomass (Table II) using the allometric model developed for this study area.

Finally, from the initial investigation and considering the diversity of tree species and growing stage of some plots, we divided the field plot biomass into two different plot settings (Table II): 1) 53-plot setting, where the maximum biomass is 532 t/ha and the forest structure and species composition of some plots are heterogeneous, and 2) 45-plot setting, where the maximum biomass is 360 t/ha and the forest structure and species composition in the plots are more homogeneous. Both plot settings were used for data analysis for all processing combinations.

TABLE III
FORMULA OF TEXTURE MEASUREMENTS USED IN THIS STUDY

Gray level co-occurrence matrix (GLCM) based texture parameter estimation "TEX"	Sum and difference histogram (SADH) based texture parameter "HISTEX"	Model-based log form texture parameter estimation "SARTEX"
1. $Mean(ME) = \sum_{i,j=0}^{N-1} i\ P_{i,j}$ 2. $Homogeneity(HO) = \sum_{i,j=0}^{N-1} i\ \frac{P_{ij}}{1+(i-j)^2}$ 3. $Contrast(CO) = \sum_{i,j=0}^{N-1} i\ P_{i,j}\ (i-j)^2$ 4. $Standard\ deviation(Std) = \sqrt{VA}$ $where\ VA == \sum_{i,j=0}^{N-1} i\ P_{i,j}\ (i-ME)^2$ 5. $Dissimilarity(DI) = \sum_{i,j=0}^{N-1} i\ P_{i,j}\ \lvert i-j\rvert$ 6. $Entropy(EN) = \sum_{i,j=0}^{N-1} i\ P_{i,j}\ (-ln\ P_{i,j})$ 7. $Angular\ Second\ Moment\ (ASM) = \sum_{i,j=0}^{N-1} i\ P_{i,j}^2$ 8. $Correlation(CR) = \sum_{i,j=0}^{N-1} i\ P_{i,j}\left[\frac{(i-ME)(j-ME)}{\sqrt{VA_i\ VA_j}}\right]$ 9. $Inverse\ Difference(ID) = \sum_{i,j=0}^{N-1} i\ \frac{P_{ij}}{\lvert i-j\rvert^2}$ 10. $GLDV\ Angular\ Second\ Moment\ (GASM) = \sum_{k=0}^{N-1} V_k^2$ 11. $GLDV\ Entropy\ (GEN) = \sum_{k=0}^{N-1} V_k\ (-ln\ V_k)$ 12. $GLDV\ Mean\ (GME) = \sum_{k=0}^{N-1} k\ V_k$ 13. $GLDV\ Contrast\ (GCO) = \sum_{k=0}^{N-1} k^2\ V_k$ Here, P (i, j) is the normalized co-occurrence matrix such that SUM (i , j=0, N-1) (P (i, j)) = 1. V(k) is the normalized grey level difference vector V(k) = SUM (i, j=0, N-1 and |i-j | = k) P (i, j)	1. $Mean\ (\mu) = \frac{\sum_{i,j} x_{ij}}{n}$ 2. $Mean\ deviation\ (MD) = \frac{\sum_{i,j} \lvert x_{ij}-\mu\rvert}{n}$ 3. $Mean\ Euclidean\ distance\ (MED) = \sqrt{\frac{\sum_{i,j}(x_{ij}-x_c)^2}{n-1}}$ 4. $Variance\ (\sigma^2) = \frac{\sum_{i,j}(x_{ij}-\mu)^2}{n-1}$ 5. $Normalized\ Coefficient\ of\ Variation(NCV) = \sqrt{\frac{\sigma^2}{\mu}}$ 6. $Skewness\ (Sk) = \frac{\sum_{i,j}(x_{ij}-\mu)^3}{(n-1)\sigma^3}$ 7. $Kurtosis\ (Ku) = \frac{\sum_{i,j}(x_{ij}-\mu)^4}{(n-1)\sigma^4}$ 8. $Energy(E) = \sum_{i,j} x_{ij}^2$ 9. $Entropy\ (H) = -\sum_{i,j} p_{ij}\ ln(p_{ij}),\ with\ p_{ij} = \frac{x_{ij}}{\sum_{i,j} x_{ij}}$ Here, x_{ij} stands for the pixel value of pixel (i, j) in the kernel over which is summed, n for the number of pixels that is summed, x_c for the kernel's center pixel value, and p_{ij} for the normalized pixel value.	1. $VI = \frac{\frac{\sum_{i,j} I_{i,j}^2}{M}}{\left[\frac{\sum_{i,j} I_{i,j}}{M}\right]^2} - 1$ 2. $VA = \frac{\frac{\sum_{i,j} I_{ij}}{M}}{\left[\frac{\sum_{i,j} A_{i,j}}{M}\right]^2} - 1$ 3. $VL = \frac{\sum_{i,j} lnI_{i,j}^2}{M} - \left[\frac{\sum_{i,j} lnI_{i,j}}{M}\right]^2$ 4. $U = \frac{\sum_{i,j} lnI_{i,j}}{M} - ln\left[\frac{\sum_{i,j} I_{i,j}}{M}\right]$ Here, I_i,j denotes the intensity of a pixel and A_i,j denotes the amplitude of a pixel

C. SAR Data Processing

1) Calculation of Backscattering Coefficient: Before texture measurement, the image was converted from digital number to a calibrated backscattering coefficient

$$\text{Calibrated value} = \frac{DN^2 + B}{A} \tag{1}$$

where "DN" is a complex number, calibrated value is the sigma nought in power, B is the offset, and A is the gain. The sigma nought in power image was then converted to scaled intensity to use as an input for texture measurement mainly because the scaled intensity image provides a better dynamic range over low backscattering targets [30]. Subsequently, conversion to sigma nought in power and sigma nought in decibels was carried out for model development.

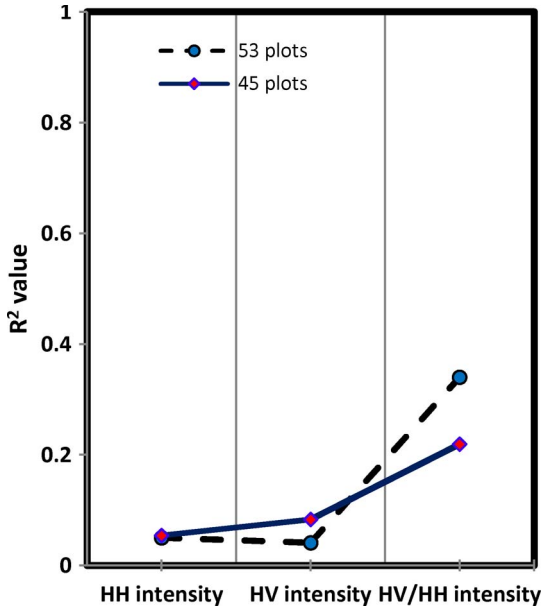

Fig. 3. Accuracy of different models using different intensity data.

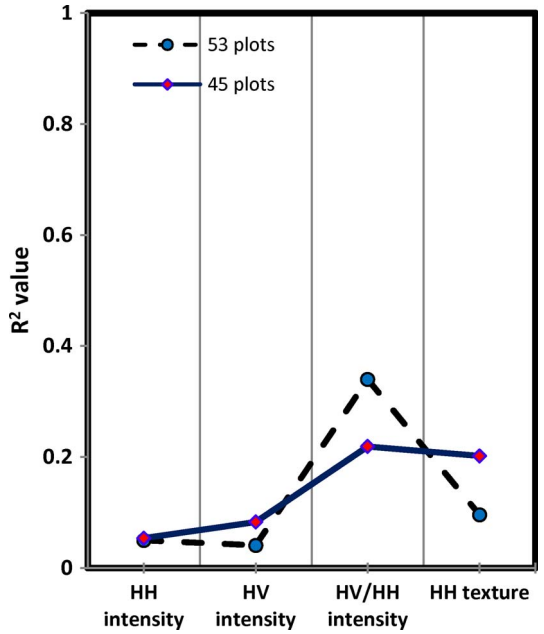

Fig. 4. Comparison of accuracy among intensity (HH, HV, and HV/HH) and HH texture parameters.

2) Texture Analysis: Image texture is characterized as the spatial variability in image tone and arises from the heterogeneity in target properties giving rise to different neighboring pixel values for the same apparent target type [28]. Several methods and techniques for describing texture based on statistical models have been developed [29]–[31]; however, three groups of texture algorithms were selected because these are commonly used, easy to implement, and can provide complementary information in the forest biomass estimation model.

The first group is the gray-level co-occurrence matrix (GLCM) [26]-based texture measurements (column 1 in Table III) which considers the relation between two neighboring pixels in one offset, as the second-order texture. In this

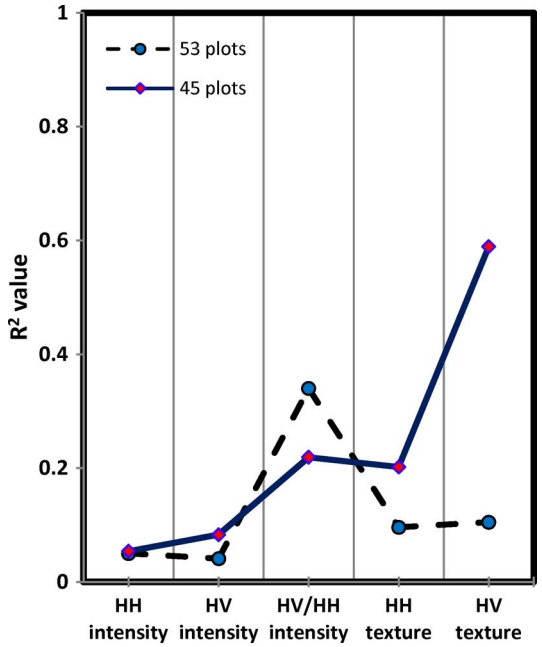

Fig. 5. Comparison of accuracy among intensity (HH, HV, and HV/HH), HH texture, and HV texture parameters.

texture algorithm, the gray value relationships in a target are transformed into the co-occurrence matrix space by a given kernel mask such as $3 * 3$, $5 * 5$, and $7 * 7$. The second group of texture algorithms (column 2 in Table III) is the sum and difference histogram (SADH) [39], where the sum and difference of two random variables with the same variances are decorrelated and the principal axes of their associated joint probability function are defined. Two maximum likelihood texture classifiers are presented depending on the type of object used for texture characterization. The third group is model-based log form texture algorithms (column 3 in Table III) reported by Oliver [40] and Oliver and Quegan [35] which presented a correlated K-distribution model for SAR image pixels with parameters defining spatial correlation lengths in x- and y-dimensions along with a spatial frequency component in one direction to model periodic variation in the autocorrelation function. Texture measures extracted by this algorithm are based on SAR-specific statistics of pixel values in the rectangular window of user-specified dimensions.

All texture algorithms were carried out using small to medium window sizes (from 3×3 to 9×9) considering the resolution of the image and the forest structure of this study area. Four texture measurement directions (0°, 45°, 90°, and 135°) were specified for the processing and texture measurements used in the research are named TEX for GLCM-based texture measurement, HISTEX for SADH-based texture parameter, SARTEX for model-based log form texture parameter, and ALLTEX for all texture classes together. The texture measurement was performed before geometric correction so that the original image resolution can be used for better texture measurement. No filtering was performed before texture measurement as there is always a tradeoff between speckle suppression and preservation of the detailed features [41].

TABLE IV
RESULTS OBTAINED FROM HV TEXTURE PARAMETERS USING DIFFERENT MODELS

Data	Model Fitting Parameters				Fitting Parameters for Intercept and Variables						
	r^2	r^2_{adj}	RMSE (t/ha)	p-level	Variables & intercept	B	Std. Err. of B	p-level	Tol	VIF	CI
Model-1 (HV ALLTEX using 53 plots)	0.105	0.069	92.15	.0620*	Intercept	154.40	33.72	.00003	-	-	-
					MD_3_HV	8551.09	3803.49	.02900	.93	1.07	3.83
					Sk_3_HV	-125.59	85.61	.14860*	.93	1.07	5.39
Model -2 (HV ALLTEX using 45 plots)	0.589	0.524	43.62	.0000	Intercept	177	58.3	.00429		-	-
					MED_3_HV	124417	19233.9	.00005	.24	4.15	3.04
					MED_9_HV	-492905	113851.5	.00011	.19	5.38	4.71
					VA_3_HV	-1103	259.0	.00013	.48	2.06	9.53
					Ori_AMP_HV	-1232	308.8	.00029	.08	12.95	14.16
					Std_9_HV	3	1.0	.01392	.21	4.81	23.34
					E_3_HV	120	49.1	.01955	.12	7.98	27.53

*indicates insignificant

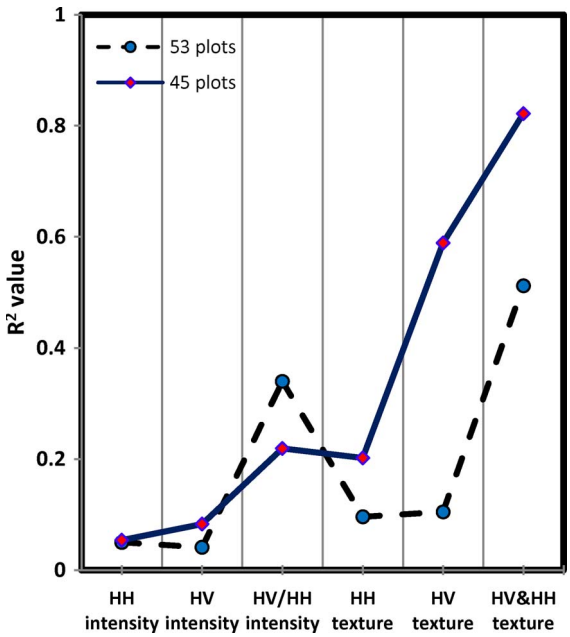

Fig. 6. Comparison of accuracy among intensity (HH, HV, and HV/HH), HH texture, HV texture, and combination of HV and HH texture parameters.

3) Geometric Correction: Geometric correction was done using Toutin's model in PCI Geomatica. A high-resolution (10 m) digital elevation model, a SPOT-5 image (as reference image), and 41 well-distributed ground control points were used for orthorectification. The rms errors in X and Y were 0.38 and 0.31, and the overall error was 0.23 pixel. All images were resampled to a 10-m pixel size because this closely approximates the real image resolution and easily matches our field plot size, and nearest neighbor resampling was used because it does not alter the statistical properties [42].

D. Statistical Analysis

The relationship between forest biomass and remotely sensed data is not easy to realize, and different techniques have already been used for this purpose such as linear regression models with or without log transformation of field biomass data [2] and multiple regression [20], [43], [44]. Nonlinear regression [16] and semiempirical models [45] have also been examined.

In this paper, a stepwise multiple linear regression approach was used to establish a relationship between SAR image parameters and field plot biomass. SAR parameters (e.g., raw intensity, texture of HV and HH, and ratio of HV and HH textures) were used as independent variables, and the plot biomass was used as the dependent variable. The best fit model was estimated, considering four common statistical parameters, namely, coefficient of determination (r^2), adjusted r^2, rmse, and p-level. However, another six statistical parameters, namely, beta coefficient, standard error of B, p-level, tolerance (Tol) [46], variance inflation factor (VIF) [20], [47], and condition index (CI) [48], were examined to avoid multicollinearity and overfitting problems. Thresholds of 0.01, > 10, and > 30 were set for Tol, VIF, and CIs, respectively, as indicators of multicollinearity.

IV. RESULTS AND ANALYSIS

A. Step-1: Intensity Images

The relationship between field biomass and simple radar intensity (HH, HV, and ratio of HV/HH) is not well defined using either 53 plots or 45 plots (Fig. 3), but the ratio of HV/HH intensity data showed better performance (adjusted $r^2 = 0.327$) than any single-polarization data. The poor result can be explained by the speckle noise in the raw (intensity) SAR data compounded by the complex forest structure and rugged topography of the study area, but most importantly, the biomass of the plots is beyond the saturation level of the raw data. As we know from previous studies, C-band SAR is likely to saturate at a low level of biomass [1], [7], [15], [22], and the biomass of all plots in this study area is above 50 t/ha (Table II).

B. Step-2: Texture Parameters for HH-Polarized Image

Almost 100 texture-derived independent variables were used step by step and altogether, to find the best fit model for biomass using both 53- and 45-plot settings, but none was found to be

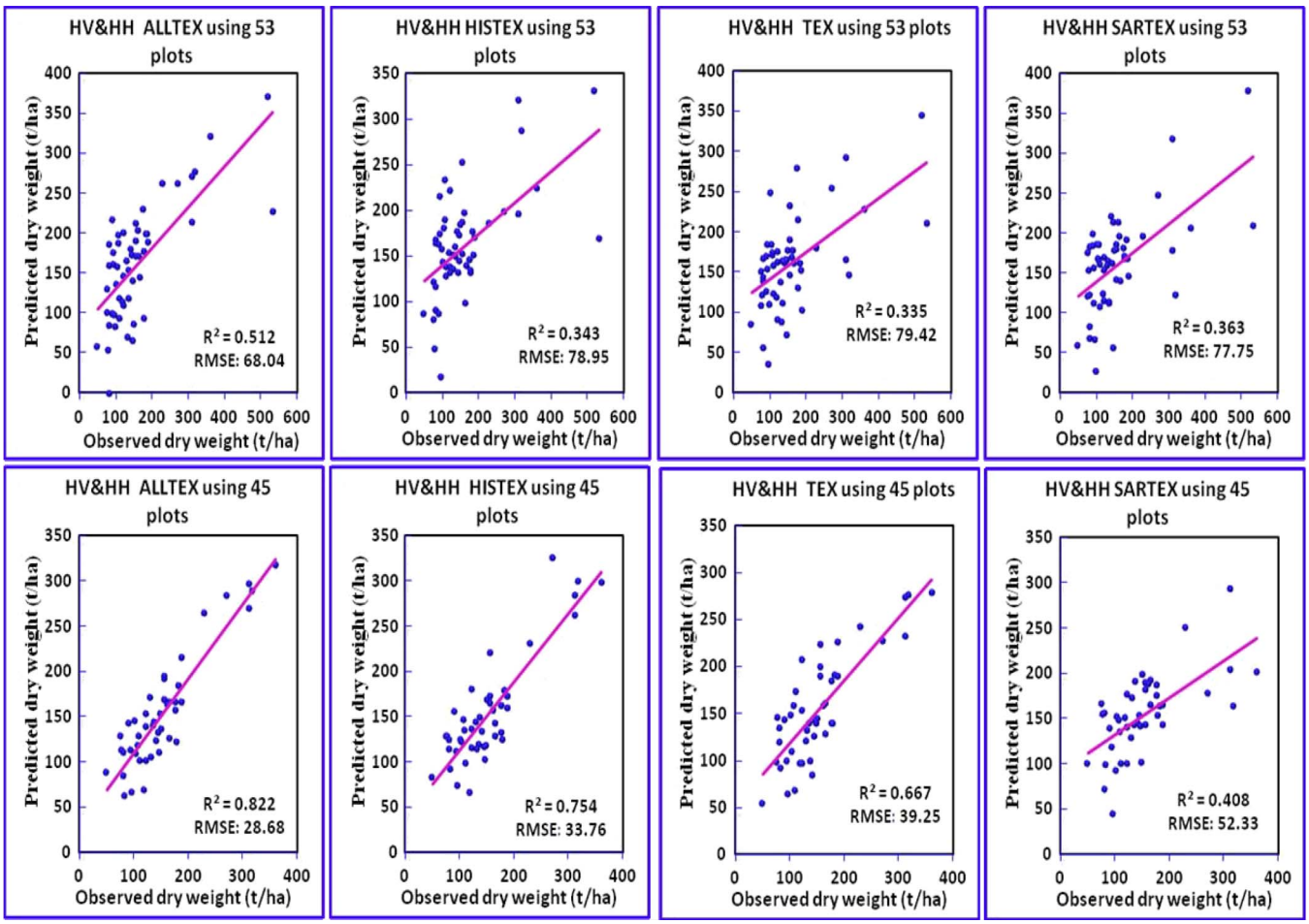

Fig. 7. Scatter plots between model-predicted biomass and observed biomass using combination of HH and HV texture data.

TABLE V
RESULTS OBTAINED FROM HH AND HV TEXTURE PARAMETERS JOINTLY USING DIFFERENT MODELS

Data	Model Fitting Parameters				Fitting Parameters for Intercept and Variables						
	r^2	r^2_{adj}	RMSE (t/ha)	p-level	Variables & intercept	B	Std. Err. of B	p-level	Tol	VIF	CI
Model-1 (HV&HH Dual with ALLTEX using 53)	0.512	0.449	68.04	.0001	Intercept	300.46	58.43	.00001	-	-	-
					GCO_5_HV	0.00	0.001	.01685	.77	1.29	3.86
					Original _AMP_HH	-491.70	94.83	.00001	.58	1.73	6.62
					μ_3_HV	3933.14	758.50	.00001	.44	2.26	7.07
					ID_5_HV	-1855.68	659.86	.00721	.43	2.35	7.85
					VA_9_HV	-827.17	315.50	.01182	.72	1.39	9.83
					ID_3_HH	690.35	324.26	.03864	.73	1.37	18.07
Model 2 (HV&HH Dual with ALLTEX using 45)	0.822	0.789	28.68	.0000	Intercept	92.34	26.36	.00122	-	-	-
					MED_3_HV	44074.08	7403.89	.00001	.23	4.32	3.30
					MED_3_HH	-7553.61	784.32	.00005	.60	1.66	4.67
					μ_3_HV	5578.61	642.63	.00005	.12	8.34	5.52
					Original HV_PW	-3260.75	495.19	.00005	.12	8.61	7.76
					ID_9_HV	-1146.27	370.004	.00371	.43	2.32	10.89
					CO_9_HH	0.01	0.002	.00369	.89	1.12	18.17
					Ku_5_HH	1.36	0.66	.04603	.93	1.07	19.34

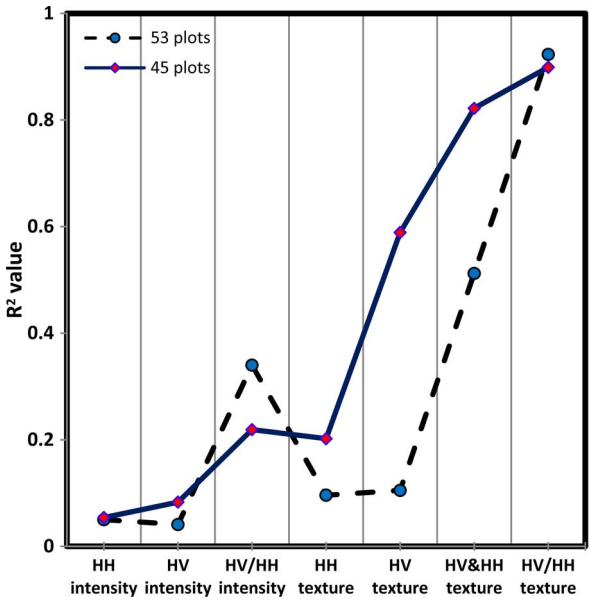

Fig. 8. Comparison of accuracy among intensity (HH, HV, and HV/HH), HH texture, HV texture, combination of HV and HH texture, and ratio of HV and HH texture parameters.

robust and can only explain about 14% (adjusted $r^2 = 0.144$ and $r^2 = 0.202$) of the variation in biomass. Using 53 plots, no texture parameters were found to be significant. On the other hand, using the 45-plot setting, TEX (adjusted $r^2 = 0.144$ and $r^2 = 0.202$) showed better performance than HISTEX and SARTEX but was equal to ALLTEX (adjusted $r^2 = 0.144$ and $r^2 = 0.202$). The goodness of fit of HH-polarized texture data was very similar to intensity of HH and HV data but was lower than the ratio of intensity images (Fig. 4). Generally, HH-polarized data are known to be less sensitive to biomass [49], [50], and after texture analysis, still poor results were obtained from the HH-polarized SAR data. It was evident that adding more and more parameters using different processing techniques was unable to significantly improve the sensitivity of HH polarization data.

C. Step-3: Texture Parameters for HV-Polarized Data

Similar to HH-polarized data processing, 100 texture parameters were used for HV data. All texture measurements (TEX, HISTEX, SARTEX, and ALLTEX) showed poor performance (with highest adjusted $r^2 = 0.07$ and $r^2 = 0.105$), and no model was found to be significant using 53 plots probably because of the higher field biomass levels represented by the 53-plot data, although it is commonly believed that HV-polarized SAR data have better sensitivity for biomass estimation [1], [7], [15], [51]. However, significant improvement (adjusted $r^2 = 0.52$) (Fig. 5 and Model-2 in Table IV) was observed using 45 plots with HV-polarized data compared to intensity (adjusted $r^2 = 0.20$) and texture of HH-polarized data (adjusted $r^2 = 0.14$). This tells us that HV-polarized SAR data have the potential to predict biomass and this can be increased using texture parameters with a goodness of fit of more than 50% using the less complex 45-plot setting.

The performance (adjusted r^2) of the different texture modules varied significantly (TEX $= 0.49$, HISTEX $= 0.28$, and SARTEX $= 0.041$), but all texture modules together (ALLTEX $= 0.52$) outperformed individual texture modules using 45 plots, probably due to each individual texture measurement providing complementary information in the model. The best model was found using all texture modules together with six variables (Model-2 in Table IV). The model, intercept, and variables were significant, but moderate multicollinearity was evident considering the set thresholds for VIF and CI. Since this best model can only define about 52% of the variability of field biomass and it also shows moderate multicollinearity effects, we decided to investigate other processing methods.

D. Step-4: Combination of Texture Parameters for HV and HH-Polarized Data

To investigate the complementarity of information from both polarizations (HH and HV), approximately 200 independent texture variables (100 from each polarization) were used. The performance of the biomass estimation increased (Figs. 6 and 7) significantly using both polarization textures jointly (HH and HV) although the magnitude of the improvement was different with respect to plot settings.

The combination of both polarized texture (HH and HV) data obtained the highest goodness of fit (adjusted r^2) of 0.449 compared with the previously obtained highest goodness of fit from intensity (0.327), texture of HH (0.079), and texture of HV (0.069) using the 53-plot setting. On the other hand, the highest goodness of fit (adjusted r^2) of 0.789 was obtained from the texture of both HH and HV polarization data using the 45-plot setting compared with previous highest accuracies of 0.201 from intensity, 0.144 from texture of HH, and 0.524 from texture of HV data. The increases in goodness of fit (Fig. 6) obtained using dual-polarization texture data are 27.17%, 82.40%, and 84.63% compared to intensity, texture of HH, and texture of HV data, respectively, using 53 plots, and 74.52%, 81.74%, and 33.58%, compared to intensity, texture of HH, and texture of HV, respectively, using 45 plots.

The performance of the individual texture modules also varied according to the number of plots used. Using 45 plots, the lowest goodness of fit ($r^2 = 0.408$ and adjusted $r^2 = 0.315$) was achieved using SARTEX, while the highest goodness of fit ($r^2 = 0.882$ and adjusted $r^2 = 0.789$) was obtained from ALLTEX (Model-2 in Table V), and the second highest goodness of fit ($r^2 = 0.75$ and adjusted $r^2 = 0.722$) was obtained from HISTEX. An almost similar pattern of goodness of fit was obtained using 53 plots, but the goodness of fit was significantly lower (highest $r^2 = 0.512$ and adjusted $r^2 = 0.449$) (Model-1 in Table V) than that for the 45-plot setting. In both plot settings, the best results were achieved from the combination of all texture modules "ALLTEX."

The best fitting model (Model-1 in Table V) using 53 plots was obtained from six independent variables, while seven independent variables (Model-2 in Table V) were used in the best fit model using 45 plots. Both models (Models 1 and 2 in Table V) are significant, and no multicollinearity effect was suspected (considering the Tol, VIF, and CI). However, the model using

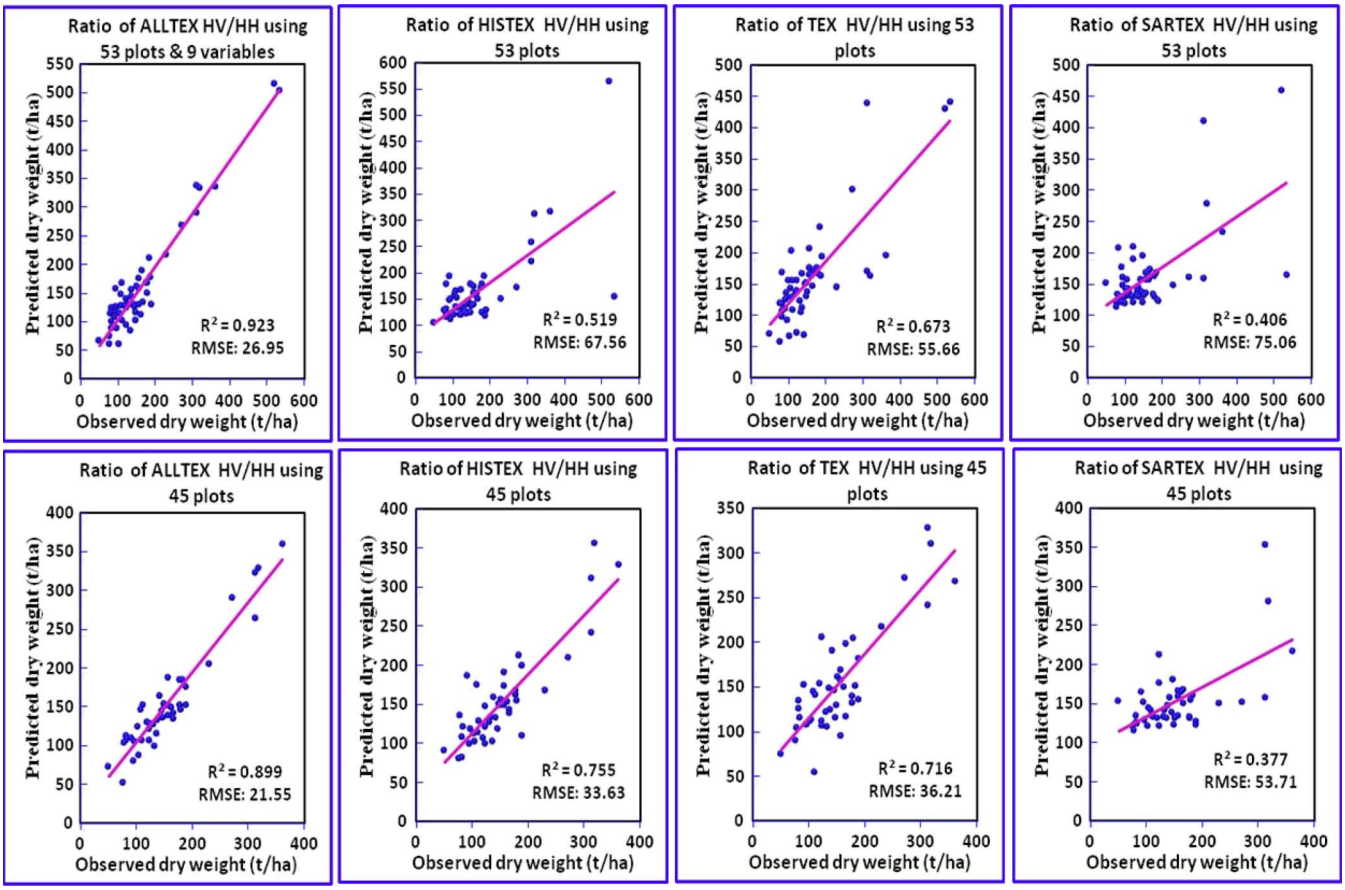

Fig. 9. Scatter plots between model-predicted biomass and observed biomass using the ratio of (HV and HH) texture data.

TABLE VI
RESULTS OBTAINED FROM THE RATIO OF TEXTURE PARAMETERS (HV/HH) USING DIFFERENT MODELS

Data	Model Fitting Parameters				Fitting Parameters for Intercept and Variables						
	r^2	r^2_{adj}	RMSE (t/ha)	p-level	Variables & intercept	B	Std. Err. of B	p-level	Tol	VIF	CI
Model-1 (Ratio of ALLTEX HV/HH using 53 plots)	.0.923	0.907	26.95	.0000	Intercept	90.04	18.56	.00002	-	-	-
					Variance_3	116.81	10.74	.00005	.30	3.34	2.48
					HO_3	1.17	0.08	.00005	.20	5.04	2.66
					ID_3	-52.05	5.43	.00005	.20	4.95	3.94
					ASM_7	55.91	11.46	.00002	.57	1.76	6.46
					MED_7	-170.05	29.91	.00001	.43	2.31	7.34
					HV/HH _ratio_PW	-8.86	2.41	.00064	.33	3.16	9.53
					μ_5	197.55	67.67	.00557	.32	3.16	10.24
					VL_3	12.85	5.43	.02264	.65	1.54	13.89
					HO_7	13.55	6.54	.04426	.40	2.49	15.66
Model-2 (Ratio of ALLTEX HV/HH using 45 plots)	0.899	0.877	21.55	.0005	Intercept	73.20	18.31	.00030	-	-	-
					Variance_3	99.33	9.39	.00005	.74	1.35	2.04
					ASM_7	62.54	8.24	.00005	.54	1.86	2.72
					HO_3	0.45	0.07	.00005	.27	3.69	3.81
					ID_3	-20.70	4.18	.00001	.25	4.07	4.57
					Ku_7	-13.09	3.73	.00123	.93	1.07	6.81
					Std_3	-7.84	2.20	.00104	.28	3.56	9.81
					GME_5	45.17	12.99	.00135	.16	6.22	10.10
					CO_7	-11.90	5.08	.02472	.26	3.83	17.35

53 plots (Model-1 in Table V) can only predict 45% of the variability of the dependent variable (DW), while the model using 45 plots (Model-2 in Table V) has the potential to estimate biomass up to 80% goodness of fit using dual-polarization SAR. Despite this high performance, we have proceeded for further investigation using the polarization ratio of texture parameters (Section IV-E) considering the potential advantages which may be realized from raw polarization ratio for minimizing forest structural effects [51] and topographic effects [52].

E. Step-5: Ratio of Texture Parameters for HV and HH-Polarized Data

At the final stage of this analysis, we used the ratio of dual-polarization (HV and HH) texture parameters because ratio is a simple image fusion/combination method which has the advantage of being unaffected by multiplicative calibration errors [35]. Furthermore, the ratio of backscattering can potentially reduce topographic effects [51], [52] and forest-type-dependent structural effects [43], [51] and thereby increase the strength of correlations [2], [53]. We assumed that the ratio of dual-polarization texture parameters may have similar advantages, resulting in an increase in the saturation level as well as an improvement of the biomass estimation. Since the ratio combines HH and HV texture parameters together, only 100 independent variables were used compared with 200 independent variables in the previous stage (Step-4 in Section IV-D).

Significant improvement was achieved for both plot settings using the ratio of texture images compared to intensity, HH texture, HV texture, and combination of HH and HV texture images (Figs. 8 and 9). The highest performance (adjusted r^2) of 0.907 and 0.877 were achieved using this ratio for the 53- (Model-1 in Table VI) and 45- (Model-2 in Table VI) plot settings, respectively. The increases in performance (Fig. 8) are 63.94%, 91.28%, 92.39%, and 50.49% compared to the best performance of intensity, HH texture, HV texture, and combined HH and HV texture images, respectively, using 53 plots, and 77.08%, 83.58%, 40.25%, and 10.03% using 45 plots. In both cases, the improvement is highly significant particularly in the case of 53 plots, where the performance improvement is really large from an adjusted r^2 of 0.449 (highest from Step-4) to 0.907.

Using the ratio of texture images, the performance of individual textures was variable, but the highest goodness of fit was achieved using all texture modules together (ALLTEX) which indicates that the different texture modules consistently provide complimentary information for biomass estimation. The ALLTEX texture model with nine independent variables (Model-2 in Table VI) achieved the highest goodness of fit (adjusted $r^2 = 0.907$ and rmse $= 26.95$ t/ha) using 53 plots. The model and all variables were significant, and all parameters for the multicollinearity test (Tol, VIF, and CI) were far below the set threshold levels. Similarly, for the 45 plots, the ALLTEX texture module achieved a highly significant result with a goodness of fit of 0.877 (adjusted r^2) and rmse of 21.55 t/ha. This model used eight independent variables (Model-1 in Table VI), and the model, intercept, and all variables are significant with no apparent multicollinearity effect.

V. Discussion

The high accuracies obtained in this analysis are promising since C-band SAR has previously been considered less effective for biomass estimation than L-band or P-band SAR but may be explained by the high quality of the data in terms of polarization, incidence angle, and spatial resolution, in combination with the many different processing techniques applied. Our finding from the raw intensity data is that backscattering of C-band SAR data is saturated at low biomass levels despite the fact that we used high-resolution data. The problem of this saturation and the reason for this are well established from many previous studies [1], [2], [7], [50].

However, the main contribution of this paper is to use the texture parameters of dual-polarization SAR in different processing steps for the estimation of forest biomass. From this endeavor, we found that, similar to raw intensity of HH polarization, texture parameters of HH polarization were less suitable for forest biomass estimation. Although we used approximately 100 texture images, the result is almost the same as for raw HH polarization. The texture parameters of HV polarization showed improvement over HH polarization texture parameters and also over raw intensity of HV polarization. The different effectiveness between the HH and HV polarization texture parameters cannot be directly compared with the findings of previous studies, but in principle, it agrees with other researchers who found that HH polarization is less sensitive for forest biomass estimation than HV polarization [1], [15], [50].

The use of texture parameters from both image channels (HH and HV) in the model jointly without ratio (i.e., HH and HV) and with ratio (i.e., HV/HV) showed substantial improvement for biomass estimation performance in both plot settings, but texture polarization ratio (adjusted $r^2 = 0.90$) greatly surpasses the performance of all other processing steps. This is a very significant improvement and indicates that the ratio of texture parameters of RADARSAT-2 dual-polarization data is very effective for biomass estimation and is adequately robust to represent the high species diversity and high biomass present in the 53-plot setting.

This image processing technique was not directly applied before for forest biomass estimation, but the basic principle, i.e., use of both polarizations together and polarization ratio, was used in many studies for land use/land cover mapping as well as forest biomass estimation, and our results agree with findings of previous researchers who found improvement from multifrequency, multipolarization, and multisensor data in the form of ratio or other combination [20], [52], [54], [55].

However, until more details are known about the interaction between forest parameters and radar backscatter, the physical interpretation of our results can only be inductive, based on our observations. While the many parameters and processing approaches examined here are unlikely to represent biomass individually, the use of multiple regression identifies the different contributions of the key components and may explain the high correlations achieved. Despite being unable to explain the result physically, we believe that the good result is an outcome of the selection of data and processing techniques together and can be explained as follows: 1) the use of dual-polarization

high-resolution C-band SAR data which are believed to be a good source of image texture; 2) the use of texture measurement which has the ability to discriminate spatial information, as well as to reduce those forest structural differences which are independent of biomass; 3) the use of complementary information from both polarization texture parameters together as this information can improve performance compared with any single-channel data; 4) the use of texture polarization ratio which gives us complementarities and advantages of reducing other effects such as forest structural differences, differences in the radar incidence angle, and topographic effects; these advantages of the use of ratio are likely to be particularly effective in our study area due to the heterogeneity of species and forest structure and complexity of the terrain; and 5) finally, the use of texture algorithms with multiple window sizes which produced uncorrelated texture parameters and this uncorrelated independent variable played an important role in the model building, explaining part of the variability of the dependent variable (field biomass).

VI. Conclusion and Recommendation

This study set out to improve forest biomass estimation from RADARSAT-2 SAR data, using intensity data and texture parameters with different data combinations. Our results suggest that the forest biomass estimation capacity of C-band can be greatly improved beyond the commonly stated saturation levels using the texture parameters of high-resolution SAR images, particularly using the ratio of texture parameters. Conclusions can be made as follows.

1) The direct relationships between C-band SAR backscattering and forest biomass are still not good for forest biomass estimation despite the use of high resolution and dual polarizations. However, texture measurement of the high-resolution C-band SAR data showed improvement particularly using HV polarization, although texture parameters of HH polarization data remain less effective and similar to the raw HH polarization data.
2) Notable improvement for forest biomass estimation can be achieved using the texture measurements of both polarizations jointly. However, the performance of this processing technique varies with the level of biomass and forest conditions and probably with topography.
3) The performance can be further improved using the texture ratio of this new C-band SAR data, and the main conclusion is that texture parameters of dual-polarization data have the potential for estimating biomass, but the ratio of polarization texture parameters has even greater potential to improve forest biomass estimation and increase saturation levels.
4) The performance of the three groups of texture measurements was inconsistent, but all texture models together outperformed all individual texture models. Although we found it difficult to make any clear recommendation as to which individual group of texture measurements is better than any other group, our suggestion is to select texture algorithms from different groups (maybe not all algorithms from all groups) in order to get complementary information in the model.
5) Finally, it is important to mention here that we obtained the best results after all of these five steps of processing and we only propose two best models (one for 45-plot setting and the other for 53-plot settings), but in fact, many models can be developed considering the number and selection of variables. We used only one study area to test our processing, but it is likely that this processing can be used in other study area as we have not used any local parameters in the model. We assume that different best models are likely to emerge in different study areas, as their texture parameters would be different, but the best model for other areas can be identified using the procedure described in this paper.

References

[1] M. C. Dobson, F. T. Ulaby, T. LeToan, A. Beaudoin, E. S. Kasischke, and N. Christensen, "Dependence of radar backscatter on coniferous forest biomass," *IEEE Trans. Geosci. Remote Sens.*, vol. 30, no. 2, pp. 412–415, Mar. 1992.
[2] K. J. Ranson and G. Sun, "Mapping biomass of a northern forest using multifrequency SAR data," *IEEE Trans. Geosci. Remote Sens.*, vol. 32, no. 2, pp. 388–396, Mar. 1994.
[3] R. A. Houghton, "Above ground forest biomass and the global carbon balance," *Global Change Biol.*, vol. 11, no. 6, pp. 945–958, Jun. 2005.
[4] D. L. Skole and C. J. Tucker, "Tropical deforestation and habitat fragmentation in the Amazon: Satellite data from 1978 to 1988," *Science*, vol. 260, no. 5116, pp. 1905–1910, Jun. 1993.
[5] Q. M. Ketterings, R. Coe, M. van Noordwijk, Y. Ambagau', and C. A. Palm, "Reducing uncertainty in the use of allometric biomass equations for predicting above-ground tree biomass in mixed secondary forests," *Forest Ecol. Manage.*, vol. 146, no. 1–3, pp. 199–209, Jun. 2001.
[6] S. Brown, A. J. R. Gillespie, and A. E. Lugo, "Biomass estimation methods for tropical forests with applications to forest inventory data," *Forest Sci.*, vol. 35, no. 4, pp. 881–902, Dec. 1989.
[7] T. Le Toan, A. Beaudoin, J. Riom, and D. Guyon, "Relating forest biomass to SAR data," *IEEE Trans. Geosci. Remote Sens.*, vol. 30, no. 2, pp. 403–411, Mar. 1992.
[8] P. S. Thenkabail, N. Stucky, B. W. Griscom, M. S. Ashton, J. Diels, B. Van der Meer, and E. Enclona, "Biomass estimations and carbon stock calculations in the oil palm plantations of African derived savannas using IKONOS data," *Int. J. Remote Sens.*, vol. 25, no. 23, pp. 5447–5472, 2004.
[9] D. Zheng, J. Rademacher, J. Chen, T. Crow, M. Bresee, J. Le Moine, and S.-R. Ryu, "Estimating aboveground biomass using Landsat 7 ETM+ data across a managed landscape in northern Wisconsin, USA," *Remote Sens. Environ.*, vol. 93, no. 3, pp. 402–411, Nov. 2004.
[10] P. Muukkonen and J. Heiskanen, "Biomass estimation over a large area based on standwise forest inventory data and ASTER and MODIS satellite data: A possibility to verify carbon inventories," *Remote Sens. Environ.*, vol. 107, no. 4, pp. 617–624, Apr. 2007.
[11] A. Garcia-Martin, F. Perez-Cabello, J. de la Riva Fernandez, and R. M. Lloveria, "Estimation of crown biomass of Pinus spp. from Landsat TM and its effect on burn severity in a Spanish fire scar," *IEEE J. Sel. Topics Appl. Earth Observ. Remote Sens.*, vol. 1, no. 4, pp. 254–265, Dec. 2008.
[12] J. E. Nichol and M. L. R. Sarker, "Improved biomass estimation using the texture parameters of two high-resolution optical sensors," *IEEE Trans. Geosci. Remote Sens.*, vol. 49, no. 3, pp. 930–948, Mar. 2011.
[13] S. Wu, "Potential application of multipolarization SAR for pine-plantation biomass estimation," *IEEE Trans. Geosci. Remote Sens.*, vol. GE-25, no. 3, pp. 403–409, May 1987.
[14] A. Luckman, J. Baker, M. Honzak, and R. Lucas, "Tropical forest biomass density estimation using JERS-1 SAR: Seasonal variation, confidence limits, and application to image mosaics," *Remote Sens. Environ.*, vol. 63, no. 2, pp. 126–139, Feb. 1998.
[15] E. Mougin, C. Proisy, G. Marty, F. Fromard, H. Puig, L. Betoulle, and J. P. Rudant, "Multifrequency and multipolarization radar backscattering from mangrove frosts," *IEEE Trans. Geosci. Remote Sens.*, vol. 37, no. 1, pp. 94–102, Jan. 1999.

[16] J. R. Santos, C. C. Freitas, L. S. Araujo, L. V. Dutra, J. C. Mura, F. F. Gama, L. S. Soler, and S. J. S. Sant'Anna, "Airborne P-band SAR applied to the aboveground biomass studies in the Brazilian tropical rainforest," *Remote Sens. Environ.*, vol. 87, no. 4, pp. 482–493, Nov. 2003.
[17] H. Wang and K. Ouchi, "Accuracy of the K-distribution regression model for forest biomass estimation by high-resolution polarimetric SAR: Comparison of model estimation and field data," *IEEE Trans. Geosci. Remote Sens.*, vol. 46, no. 4, pp. 1058–1064, Apr. 2008.
[18] F. Garestier and T. Le Toan, "Estimation of the backscatter vertical profile of a pine forest using single baseline P-band (Pol-)InSAR data," *IEEE Trans. Geosci. Remote Sens.*, vol. 48, no. 9, pp. 3340–3348, Sep. 2010.
[19] Z. J. Bortolot and R. H. Wynne, "Estimating forest biomass using small footprint LiDAR data: An individual tree-based approach that incorporates training data," *ISPRS J. Photogramm. Remote Sens.*, vol. 59, no. 6, pp. 342–360, 2005.
[20] P. Hyde, R. Nelson, D. Kimes, and E. Levine, "Exploring LiDAR–RaDAR synergy—predicting aboveground biomass in a Southwestern Ponderosa pine forest using LiDAR, SAR and InSAR," *Remote Sens. Environ.*, vol. 106, no. 1, pp. 28–38, Jan. 2007.
[21] J. Amini and J. T. S. Sumantyo, "Employing a method on SAR and optical images for forest biomass estimation," *IEEE Trans. Geosci. Remote Sens.*, vol. 47, no. 12, pp. 4020–4026, Dec. 2009.
[22] M. L. Imhoff, "Radar backscatter and biomass saturation: Ramification for global biomass inventory," *IEEE Trans. Geosci. Remote Sens.*, vol. 33, no. 2, pp. 511–518, Mar. 1995.
[23] F. T. Ulaby, F. Kouyate, B. Brisco, and T. H. L. Williams, "Textural information in SAR images," *IEEE Trans. Geosci. Remote Sens.*, vol. GE-24, no. 2, pp. 235–245, Mar. 1986.
[24] F. Dell'Acqua and P. Gamba, "Texture-based characterization of urban environments on satellite SAR images," *IEEE Trans. Geosci. Remote Sens.*, vol. 41, no. 1, pp. 153–159, Jan. 2003.
[25] I. Champion, P. Dubois-Fernandez, D. Guyon, and M. Cottrel, "Radar image texture as a function of forest stand age," *Int. J. Remote Sens.*, vol. 29, no. 6, pp. 1795–1800, Mar. 2008.
[26] R. M. Haralick, K. Shanmugam, and I. Dinstein, "Textural features for image classification," *IEEE Trans. Syst., Man, Cybern.*, vol. smc 3, no. 6, pp. 610–621, Nov. 1973.
[27] C. E. Woodcock and A. H. Strahler, "The factor of scale in remote sensing," *Remote Sens. Environ.*, vol. 21, no. 3, pp. 311–332, Apr. 1987.
[28] A. J. Luckman, A. C. Frery, C. C. F. Yanasse, and G. B. Groom, "Texture in airborne SAR imagery of tropical forest and its relationship to forest regeneration stage," *Int. J. Remote Sens.*, vol. 18, no. 6, pp. 1333–1349, 1997.
[29] T. M. Kuplich, P. J. Curran, and P. M. Atkinson, "Relating SAR image texture to the biomass of regenerating tropical forests," *Int. J. Remote Sens.*, vol. 26, no. 21, pp. 4829–4854, Nov. 2005.
[30] E. Podest and S. Saatchi, "Application of multiscale texture in classifying JERS-1 radar data over tropical vegetation," *Int. J. Remote Sens.*, vol. 23, no. 7, pp. 1487–1506, Apr. 2002.
[31] R. J. Dekker, "Texture analysis and classification of ERS SAR images for map updating of urban areas in the Netherlands," *IEEE Trans. Geosci. Remote Sens.*, vol. 41, no. 9, pp. 1950–1958, Sep. 2003.
[32] D. Chen, D. A. Stow, and P. Gong, "Examining the effect of spatial resolution and texture window size on classification accuracy: An urban environment case," *Int. J. Remote Sens.*, vol. 25, no. 11, pp. 2177–2192, Jun. 2004.
[33] D. Lu, "Aboveground biomass estimation using Landsat TM data in the Brazilian Amazon," *Int. J. Remote Sens.*, vol. 26, no. 12, pp. 2509–2525, Jun. 2005.
[34] K. L. Castro, G. A. Sanchez-Azofeifa, and B. Rivard, "Monitoring secondary tropical forests using space-borne data: Implications for Central America," *Int. J. Remote Sens.*, vol. 24, no. 9, pp. 1853–1894, Jan. 2003.
[35] C. Oliver and S. Quegan, *Understanding Synthetic Aperture Radar Images*. Raleigh, NC: SciTech Publication, 2004, p. 479.
[36] J. P. M. Overman, H. J. L. Witte, and J. G. Saldarriaga, "Evaluation of regression models for above-ground biomass determination in Amazon rainforest," *J. Trop. Ecol.*, vol. 10, no. 2, pp. 207–218, May 1994.
[37] C. B. M. Arevalo, T. A. Volk, E. Bevilacqua, and L. Abrahamson, "Development and validation of aboveground biomass estimations for four Salix clones in central New York," *Biomass Bioenergy*, vol. 31, no. 1, pp. 1–12, Jan. 2006.
[38] G. L. Baskerville, "Use of logarithmic regression in the estimation of plant biomass," *Can. J. Forest Res.*, vol. 2, no. 1, pp. 49–53, Mar. 1972.
[39] M. Unser, "Sum and difference histograms for texture classification," *IEEE Trans. Pattern Anal. Mach. Intell.*, vol. PAMI-8, no. 1, pp. 118–125, Jan. 1986.
[40] C. J. Oliver, "Optimum texture estimators for SAR clutter," *J. Phys. D, Appl. Phys.*, vol. 26, no. 11, pp. 1824–1835, Nov. 1993.
[41] A. N. Nyoungui, E. Tonye, and A. Akono, "Evaluation of speckle filtering and texture analysis methods for land cover classification from SAR images," *Int. J. Remote Sens.*, vol. 23, no. 9, pp. 1895–1925, Jan. 2002.
[42] G. M. Foody, D. S. Boyd, and M. E. J. Cutler, "Predictive relations of tropical forest biomass from Landsat TM data and their transferability between regions," *Remote Sens. Environ.*, vol. 85, no. 4, pp. 463–474, Jun. 2003.
[43] M. C. Dobson, F. T. Ulaby, L. E. Pierce, T. L. Sharik, K. M. Bergen, J. Kellndorfer, J. R. Kendra, E. Li, Y. C. Lin, A. Nashashibi, K. Sarabandi, and P. Siqueira, "Estimation of forest biophysical characteristics in northern Michigan with SIR-C/X-SAR," *IEEE Trans. Geosci. Remote Sens.*, vol. 33, no. 4, pp. 877–895, Jul. 1995.
[44] P. A. Townsend, "Estimating forest structure in wetlands using multitemporal SAR," *Remote Sens. Environ.*, vol. 79, no. 2/3, pp. 288–304, Feb. 2002.
[45] T. Castel, F. Guerra, Y. Caraglio, and F. Houllier, "Retrieval biomass of a large Venezuelan pine plantation using JERS-1 SAR data. Analysis of forest structure impact on radar signature," *Remote Sens. Environ.*, vol. 79, no. 1, pp. 30–41, Jan. 2002.
[46] D. A. Belsley, E. Kuh, and R. E. Welsch, *Regression Diagnostics: Identifying Influential Data and Sources of Collinearity*. New York: Wiley, 1980, p. 292.
[47] M. H. Kutner, C. J. Nachtsheim, J. Neter, and W. Li, *Applied Linear Statistical Models*, vol. 5th. Boston, MA: McGraw-Hill Irwin, 2005, p. 1396.
[48] C. M. Douglas, E. A. Peck, and G. G. Vining, *Introduction to Linear Regression Analysis*, vol. 4th. Hoboken, NJ: Wiley, 2006.
[49] E. Rignot, J. Way, C. Williams, and L. Viereck, "Radar estimates of aboveground biomass in boreal forests of interior Alaska," *IEEE Trans. Geosci. Remote Sens.*, vol. 32, no. 5, pp. 1117–1124, Sep. 1994.
[50] E. S. Kasischke, N. L. Christensen, Jr., and L. L. Bourgeau-Chavez, "Correlating radar backscatter with components of biomass in loblolly pine forests," *IEEE Trans. Geosci. Remote Sens.*, vol. 33, no. 3, pp. 643–659, May 1995.
[51] K. J. Ranson, S. Saatchi, and G. Sun, "Boreal forest ecosystem characterization with SIR-C/XSAR," *IEEE Trans. Geosci. Remote Sens.*, vol. 33, no. 4, pp. 867–876, Jul. 1995.
[52] J. Shi and J. Dozier, "Mapping seasonal snow with SIR-C/X-SAR in mountainous areas," *Remote Sens. Environ.*, vol. 59, no. 2, pp. 294–307, Feb. 1997.
[53] G. M. Foody, R. M. Green, R. M. Lucas, P. J. Curran, M. Honzak, and I. Do Amaral, "Observations on the relationship between SIR-C radar backscatter and the biomass of regenerating tropical forests," *Int. J. Remote Sens.*, vol. 18, no. 3, pp. 687–694, Feb. 1997.
[54] P. A. Harrell, E. S. Kasischke, L. L. Bourgeau-Chavez, E. M. Haney, and N. L. Christensen, Jr., "Evaluation of approaches to estimating aboveground biomass in southern pine forests using SIR-C data," *Remote Sens. Environ.*, vol. 59, no. 2, pp. 223–233, Feb. 1997.
[55] J. E. S. Fransson and H. Israelsson, "Estimation of stem volume in boreal forests using ERS-1 C- and JERS-1 L-band SAR data," *Int. J. Remote Sens.*, vol. 20, no. 1, pp. 123–137, Jan. 1999.

Md. Latifur Rahman Sarker was born in Gaibandha, Bangladesh, in 1968. He received the M.S. degree in geodesy and geoinformatics from the Royal Institute of Technology (KTH), Stockholm, Sweden, in 2005 and the Ph.D. degree in biomass estimation using remote sensing techniques from The Hong Kong Polytechnic University, Kowloon, Hong Kong, in 2010.

He is currently a Senior Lecturer with the Department of Remote Sensing, Universiti Teknologi Malaysia, Johor Bahru, Malaysia. He is also with the Department of Geography and Environmental Studies, University of Rajshahi, Rajshahi, Bangladesh. His research interests involve the application of optical and synthetic aperture radar (SAR) data for land use/land cover mapping and biomass estimation, vegetation mapping, wavelet image fusion of SAR and optical data, texture processing, artificial neural network, water and air quality monitoring, and feature extraction.

Janet Nichol received the B.Sc. degree from the University of London, London, U.K., the M.A. degree from the University of Colorado, Boulder, and the Ph.D. degree from Aston University, Birmingham, U.K.

She subsequently worked in the U.K., Nigeria, Singapore, and the Republic of Ireland. Since 2001, she has taught and undertaken research at the Department of Land Surveying and Geo-Informatics, The Hong Kong Polytechnic University, Kowloon, Hong Kong. She has background in physical geography, with specialization in remote sensing, and ecology. She has published over 80 peer-reviewed journal papers and several book chapters and acted as Editor and Reviewer for many scientific journals. Her research interests are in the application of remote sensing techniques to environmental assessment and monitoring, including urban climate and climate change, quaternary climate change, vegetation mapping, air quality monitoring, and aspects of image processing.

Huseyin Baki Iz received the Ph.D. degree from the Geodetic Science Department, The Ohio State University, Columbus, in 1987.

He is currently a Professor of geodetic science and spatial analysis with the Department of Land Surveying and Geo-Informatics, The Hong Kong Polytechnic University, Kowloon, Hong Kong. His recent research interests involve global mean sea level variations, kinematic geodesy, and selenodesy.

Baharin Bin Ahmad received the B.Sc. degree from Newcastle University, Newcastle upon Tyne, U.K., the M.Sc. degree from the Curtin University of Technology, Perth, Australia, and the Ph.D. degree from the University of New South Wales, Sydney, Australia.

He is currently teaching in the Department of Remote Sensing, Universiti Teknologi Malaysia, Johor Bahru, Malaysia. He has background in surveying science, with specialization in remote sensing. His recent research interests involve application of radar data, forest encroachment mapping, and landslide susceptibility mapping.

Alias Abdul Rahman received the M.Sc. degree from ITC, Enschede, The Netherlands, in 1992 and the Ph.D. degree from the University of Glasgow, Glasgow, U.K., in 2000.

He is currently a Professor of 3-D geographic information system (GIS) with Universiti Teknologi Malaysia, Johor Bahru, Malaysia, where he is also an Academic Staff Member and the Dean of the Faculty of Geoinformation and Real Estate. He also gives lecture at Stuttgart Technology University of Applied Sciences, Stuttgart, Germany; Yildiz Technical University, Istanbul, Turkey; Technische Universiteit Delft, Delft, The Netherlands; and UNESCO-IHE, Delft. His main research interest is 3-D GIS. He has produced two books with Springer Verlag and more than 100 technical papers on the subject and other related subjects.

Dr. Rahman is currently the Chair of Working Group II/5 "Multidimensional and Mobile Data Models" of Commission II of the International Society for Photogrammetry and Remote Sensing.